J Physiol 586.24 (2008) pp 5911–5929

The Journal of Physiology

Role of the hyperpolarization-activated current I_h in somatosensory neurons

Aliakmal Momin[1], Hervé Cadiou[1], Adrian Mason[2] and Peter A. McNaughton[1]

[1] *Department of Pharmacology, University of Cambridge, Cambridge, CB2 1PD, UK*
[2] *Department of Molecular Pharmacology, Schering-Plough Corp, Newhouse, Lanarkshire ML1 5SH, UK*

The hyperpolarization-activated current (I_h) is an inward current activated by hyperpolarization from the resting potential and is an important modulator of action potential firing frequency in many excitable cells. Four hyperpolarization-activated, cyclic nucleotide-modulated subunits, HCN1–4, can form I_h ion channels. In the present study we investigated the function of I_h in primary somatosensory neurons. Neuronal firing in response to current injection was promoted by elevating intracellular cAMP levels and inhibited by blockers of I_h, suggesting that I_h plays a critical role in modulating firing frequency. The properties of I_h in three size classes of sensory neurons were next investigated. In large neurons I_h was fast activating and insensitive to elevations in cAMP, consistent with expression of HCN1. I_h was ablated in most large neurons in HCN1$^{-/-}$ mice. In small neurons a slower activating, cAMP-sensitive I_h was observed, as expected for expression of HCN2 and/or HCN4. Consistent with this, I_h in small neurons was unchanged in HCN1$^{-/-}$ mice. In a neuropathic pain model HCN1$^{-/-}$ mice exhibited substantially less cold allodynia than wild-type littermates, suggesting an important role for HCN1 in neuropathic pain. This work shows that I_h is an important modulator of action potential generation in somatosensory neurons.

(Received 9 September 2008; accepted after revision 15 October 2008; first published online 20 October 2008)
Corresponding author P. A. McNaughton: Department of Pharmacology, University of Cambridge, Tennis Court Road, Cambridge CB2 1PD, UK. Email: pam42@cam.ac.uk

The intensity of sensation in all sensory systems is determined mainly by the frequency of action potential firing in afferent nerve fibres. This generalization also holds true for sensory afferents responding to painful stimuli, named nociceptors by Sherrington (1906). Nociceptors are unique amongst sensory receptors, though, in that the sensitivity of the nerve terminals to noxious stimuli is enhanced in inflammatory hyperalgesia, which is caused by the release of pro-inflammatory mediators such as bradykinin, nerve growth factor (NGF) and prostaglandin E_2 (PGE_2). Pro-inflammatory mediators increase the frequency of action potentials elicited by a noxious stimulus by two distinct mechanisms: by increasing the inward current activated by a noxious stimulus, or by increasing the frequency of action potentials elicited by a given inward current. We focus here on the second process.

Three mechanisms have been proposed to explain the modulation of action potential generation by pro-inflammatory mediators. The threshold for activation of the voltage-sensitive sodium channel $Na_V1.8$ is shifted in the negative direction by phosphorylation by PKA and/or PKC (Gold *et al.* 1996, 1998; England *et al.* 1996; Fitzgerald *et al.* 1999). This mechanism seems unlikely to offer a complete explanation of either inflammatory hyperalgesia or neuropathic pain, however, because in $Na_V1.8^{-/-}$ mice inflammatory hyperalgesia is reduced but not abolished, and neuropathic pain is unaffected (Akopian *et al.* 1999; Kerr *et al.* 2001). Secondly, a voltage-sensitive K^+ current is inhibited by activation of PKA (Nicol *et al.* 1997; Evans *et al.* 1999; Jiang *et al.* 2003). Finally, the voltage dependence of activation of the hyperpolarization-activated inward current, I_h, is shifted to less negative membrane potentials (Ingram & Williams, 1994, 1996).

I_h was first studied in cardiac pacemaker cells (DiFrancesco & Ojeda, 1980; DiFrancesco, 1993). I_h is activated by *hyperpolarization* from the resting potential, rather than by depolarization as for other ion channels. The activation range of I_h is shifted in the positive direction by a direct binding of adenosine 3′,5′-cyclic monophosphate (cAMP) to a cyclic-nucleotide binding region located in the C-terminal cytoplasmic domain (DiFrancesco & Tortora, 1991; Kaupp & Seifert, 2001), thereby increasing the inward current activated by

This paper has online supplemental material.

DOI: 10.1113/jphysiol.2008.163154

hyperpolarization. I_h is also expressed in many neurons, where its presence can modulate the resting potential and the action potential firing frequency (Pape & McCormick, 1989; Pape, 1996; Ludwig *et al.* 2003; Nolan *et al.* 2003; Chan *et al.* 2004).

Four ion channel subunits responsible for I_h have been cloned and are termed hyperpolarization-activated, cyclic nucleotide-modulated (HCN1–4) channels (reviewed by Kaupp & Seifert, 2001). HCN channels expressed as homomers differ in two main respects: the activation time constants are in the order of HCN1 < HCN2 < HCN3 < HCN4; and HCN2 and HCN4 are strongly modulated by elevations in cAMP, with the midpoint of the voltage-activation curve shifted in the positive direction by 12–20 mV, whereas HCN1 and HCN3 channels show little sensitivity to cAMP. These differences can be used as a guide to determining the molecular makeup of I_h in dorsal root ganglion (DRG) neurons.

Here we studied the properties of I_h in primary sensory neurons, the role of I_h in the initiation of action potential firing, and the role of one isoform, HCN1, in inflammatory and neuropathic pain. Initial studies were carried out in sensory neurons from neonatal rat, and we then confirmed that I_h had similar properties in sensory neurons from adult mice. We found that I_h plays a critical role in the enhanced generation of action potentials caused by PGE_2. We show that I_h has different properties in large non-nociceptive neurons, which express a fast, cAMP-insensitive I_h consistent with expression of HCN1, and in small nociceptive neurons, which express a slower, cAMP-sensitive I_h. I_h was found to be absent in large neurons from $HCN1^{-/-}$ mice. Finally, the role played by HCN1 in inflammatory and neuropathic pain *in vivo* was investigated by comparing thermal and mechanical thresholds in $HCN1^{+/+}$ and $HCN1^{-/-}$ mice.

Methods

Animal experiments

All experiments performed on animals were carried out in accordance with the Animal Scientific Procedures Act of the United Kingdom (Section 1, revised 1986) and were monitored by the Home Office. Permission to carry out the procedures as described below was granted by an institutional ethical review committee.

Cell culture

Rat dorsal root ganglion (DRG) neurons. DRG neurons were isolated from neonatal Wistar rats (3–7 days old) killed by cervical dislocation followed by decapitation. DRG neurons were prepared as previously described (Cesare & McNaughton, 1996). Briefly, 20–30 ganglia were isolated from the full length of the spinal column following removal of the spinal cord. After incubation in collagenase (12.5 mg ml^{-1}) for 1 h at 37°C, ganglia were mechanically triturated with fire-polished glass Pasteur pipettes. The cell suspension was centrifuged and re-suspended in Dulbecco's modified Eagle's medium (DMEM, Gibco) supplemented with 50 u ml^{-1} penicillin and 0.05 mg ml^{-1} streptomycin (Invitrogen), 1% L-glutamine (Invitrogen), 10% fetal bovine serum (FBS, Gibco), 50 ng ml^{-1} nerve growth factor (NGF, Promega) and 1.25 μg ml^{-1} cytosine β-D-arabinofuranoside (Ara-C, Sigma). DRG neurons were plated onto 35 mm Petri dishes previously coated with poly L-lysine (20 μg ml^{-1}, Sigma). After 24 h the medium was replaced with DMEM supplemented with 1% N-2 supplement Invitrogen, 50 ng ml^{-1} NGF and 0.5 μg ml^{-1} Ara-C. All electrophysiology recordings were made within 48 h of dissociation. DRG neurons were classified based on diameter of somata as follows: small (< 25 μm), medium (25–35 μm) and large (> 35 μm).

Mouse DRG neurons. DRG neurons were isolated as above from $HCN1^{+/+}$ and $HCN1^{-/-}$ adult mice killed by cervical dislocation and prepared using a standard enzymatic dissociation procedure. Briefly, ganglia were incubated in papain (20 units ml^{-1}, Sigma) for 20 min at 37°C followed by collagenase/dispase (5 mg ml^{-1}, Invitrogen, and 12 mg ml^{-1}, Roche, respectively) for 20 min at 37°C. Ganglia were then mechanically triturated. The resultant cell suspension was layered onto 25% Percoll in L15 (Sigma) and was centrifuged at 1030 *g* for 8 min. Neurons were re-suspended in F12 media (Gibco) supplemented with 10% heat-inactivated horse serum (Invitrogen), 100 u ml^{-1} penicillin and 0.1 mg ml^{-1} streptomycin (Sigma) and 50 ng ml^{-1} NGF (Invitrogen). DRG neurons were plated onto 13 mm cover-slips previously coated with poly L-lysine (50 μg ml^{-1}, Sigma) and laminin (30 μg ml^{-1}, Invitrogen). All electrophysiological recordings were made within 48 h of dissociation. Mouse DRG neurons were classified based on diameter of somata as follows: small (< 20 μm), medium (20–30 μm) and large (> 30 μm).

Electrophysiology

Solutions. Extracellular solution contained (in mM): 140 NaCl, 1.8 $CaCl_2$, 1 $MgCl_2$, 4 KCl, 10 Hepes, 4 D(+)glucose, adjusted to pH 7.4 with NaOH, osmolarity 300–310 mosmol l^{-1}. Pipettes were filled with an intracellular solution containing (in mM): 140 KCl, 1.6 $MgCl_2$, 2 EGTA, 2.5 MgATP, 0.5 Li_2GTP, 10 Hepes and adjusted to pH 7.3 with KOH, osmolarity 310–315 mosmol l^{-1}. Cells were continuously perfused with extracellular solution using a gravity-fed perfusion system.

Current-clamp and voltage-clamp recordings. Current-clamp and voltage-clamp experiments were performed using an Axopatch 200B patch-clamp amplifier (MDS, CA, USA). Pipettes, resistance 3–6 MΩ, were pulled from Blaubrand 100 μl borosilicate glass micropipettes (Scientific Laboratory Supplies) using Brown-Flaming P-80 and P-97 horizontal micropipette pullers (Sutter Instruments) and in some instances were fire-polished to improve sealing. All experiments were begun in voltage-clamp mode. Pipette capacitance transients were cancelled while in cell-attached mode and whole-cell capacitance (10–40 pF) and series resistance (70–80%) were compensated once whole-cell mode had been attained. Pipette liquid junction potentials were calculated to be −3.7 mV using pCLAMP software and all values of membrane potential have been corrected using this value. Whole-cell membrane currents and voltages were filtered at 1 kHz and sampled at 10 kHz. Data were acquired and analysed using either pCLAMP 9.0 software (MDS, CA, USA) or Signal 2.16 (Cambridge Electronic Design). All recordings were made at 22–24°C.

In current-clamp experiments action potential firing in small rat DRG neurons was elicited by a series of depolarizing current pulses (5 s duration) from 0 to 200 pA in 50 pA step increments. I_h was identified in these neurons by the presence of voltage 'sag' of greater than 10% following injection of a hyperpolarizing current pulse of 500 pA (see Fig. 1*A*), and neurons expressing I_h were chosen for further testing. The fast current-clamp mode was employed in order to minimize artifacts which can be introduced into recordings of rapidly changing voltage signals (Magistretti *et al.* 1998). In the fast current-clamp mode the 10–90% step response rise time is 10 μs with cell parameters similar to those of small DRG neurons (Axopatch 200B manual). The most rapidly changing signal in the present experiments is the rising phase of the action potential, which in small DRG neurons has a rate of rise ∼40 V s^{-1} (see Fig. 1*D*). At the point of fastest rate of rise of the action potential, 40 mV positive to the resting potential, the maximum voltage error introduced by the 10 μs delay will be *ca* 1%. The error will be less for other more slowly changing voltage signals. We conclude that negligible distortion of the voltage signal will be introduced.

I_h was studied in voltage-clamp recordings in rat and mouse DRG neurons using a series of depolarizing and hyperpolarizing step voltage pulses. Rat DRG neurons were subjected to voltage-clamp steps from a holding potential of −60 mV to between −20 and −160 mV for 2 s in 10 mV increments, followed by a final step to −160 mV for 1 s. A similar hyperpolarizing voltage protocol was used to activate I_h in mouse HCN1$^{+/+}$ and HCN1$^{-/-}$ DRG neurons, except that mouse neurons were less able to withstand extreme hyperpolarization and so were pulsed to a maximum membrane potential of −140 mV.

I_h currents recorded in voltage-clamp mode were found to be contaminated by a rapidly decaying inward current (Scroggs *et al.* 1994; Yagi & Sumino, 1998; Komagiri & Kitamura, 2003). To remove this interfering current and to reveal 'pure' I_h, a second series of identical voltage steps was imposed following inhibition of I_h using the fast-acting and reversible I_h blocker CsCl (5 mM) and these traces were then subtracted from the raw traces to give Cs-subtracted traces (Mo & Davis, 1997; Southan *et al.* 2000) (see Fig. 3). This procedure was adopted for all traces apart from those shown in Fig. 5.

We investigated whether the standard 2 s pulse was adequate to allow I_h current to reach steady state at all membrane potentials by comparing activation curves obtained with a variable-length pulse protocol (cf. Altomare *et al.* 2003) in which pulse lengths up to 20 s in length were imposed. For small HCN1$^{+/+}$ mouse neurons, in which activation of I_h is slowest, the extended pulse length gave a less steep activation curve and a value of $V_{1/2}$ shifted to more positive potentials by 6 mV. The extended pulse protocol was, however, protracted and its use was impractical when several activation curves needed to be determined in quick succession in different solutions. We also note that *shifts* in voltage-activation curves, a main focus of this paper, are much less affected than the *absolute* positions of voltage-activation curves by incomplete activation of I_h.

The voltage dependence of activation and therefore the mid-point potential ($V_{1/2}$) of I_h was obtained from tail currents derived upon a final step to either −160 mV (rat) or −140 mV (mouse). Activation curves were fitted with a Boltzmann equation of the following form:

$$I_t/I_{t(max)} = 1/(1 + \exp[(V_m - V_{1/2})/k]),$$

where V_m is the membrane potential of the prepulse, $V_{1/2}$ is the membrane potential at which I_h is half-activated, k is the slope factor, I_t is the current amplitude of the tail current recorded for a given prepulse and $I_{t(max)}$ is the maximum current amplitude of the tail current. Values of $V_{1/2}$ were found to stabilize within 5 min of attaining whole-cell mode and all recordings were made after at least this interval. The rate of channel activation was found to be well fitted in all cases with a double exponential function (Santoro *et al.* 2000). Time constants were determined by fitting currents using pCLAMP or Signal software with a double-exponential function of the form:

$$I_h(t) = A_f \exp(-t/\tau_f) + A_s \exp(-t/\tau_s),$$

where $I_h(t)$ is the amplitude of the current at time t and A_f and A_s are the initial amplitudes of the fast (τ_f) and slow (τ_s) activation time constant components, respectively.

Generation of HCN1$^{-/-}$ mice

HCN1 conditional knockout mice were generated by homologous recombination in embryonic stem cells. This work was carried out for us by Lexicon Pharmaceuticals, Inc. Exon1, encoding the cytoplasmic amino tail of the HCN1 protein, was flanked with LoxP sites (see Fig. S1*A* in online Supplemental material). A phosphoglycerate kinase (PGK) promoter-driven neomycin resistance (Neo) gene was inserted between exon1 and the downstream LoxP site. Homologous recombination was confirmed by Southern blot analysis (Supplemental Fig. S1*B*). Using a 3′ external probe, a 20 kb *Eco*R I fragment could be detected in wild-type mice, whereas mice carrying both wild-type and the targeted allele gave rise to the expected 20 kb and 7 kb fragments. HCN1 knockout mice (HCN1$^{-/-}$) were subsequently generated by mating mice carrying the LoxP-targeted allele (flox mice) with a global deleter strain, expressing Cre under the cyto-megalovirus (CMV) promoter (Jackson Labs). Deletion of exon1 was confirmed by PCR on genomic DNA from tail biopsies (Supplemental Fig. S1*B*). HCN1$^{-/-}$ mice were viable, fertile and obtained in the expected Mendelian ratios. To confirm the absence of HCN1 mRNA, RT-PCR experiments were performed on RNA isolated from a range of tissues from both knockout and wild-type littermate mice. Primers spanning exon1–2, 2–3 and 4–5 were used to detect HCN1 mRNA. Whereas in wild-type mice HCN1 transcripts were present in brain, eye, tongue and heart (Supplemental Fig. S2*B*; only RT-PCR exon2–3 is shown), no transcripts could be detected in tissues of the HCN1$^{-/-}$ mice. An N-terminal HCN1 antibody detected a 96 kDa protein in wild-type brain and spleen (not in heart, eye and tongue) that was not present in the HCN1$^{-/-}$ protein samples (Supplemental Fig. S2*A*).

For both electrophysiological and behavioural experiments heterozygous HCN1$^{+/-}$ mice were produced by back-crossing onto the parental strain for six generations and were mated. HCN1$^{+/+}$ and HCN1$^{-/-}$ littermates were identified from PCR on genomic DNA from tail biopsies and were used for experiments.

Behavioural studies

Animals were allowed free access to food and water and were kept in a 12 h on, 12 h off light–dark cycle. All behavioural experiments were performed in a temperature-controlled environment ($24 \pm 1^{\circ}$C) with humidity of 45–55%. Adult mice of both sexes were used, weighing between 20 and 30 g and age matched. In all cases mice were given 1 h to habituate to the test environment before experimentation commenced.

Inflammatory pain. Inflammatory pain was induced by the administration of 0.75 nmol PGE_2 in 20 μl saline solution into the plantar surface of the hind paw. Saline was injected in control animals. Latencies of paw withdrawal from a mechanical and heat stimulus (see below) were recorded at 0.5, 1, 2 and 24 h after injection.

Partial sciatic nerve ligation (Seltzer model). Partial sciatic nerve ligation (PNL) was performed under iso-flurane anaesthesia (administered at 3% and maintained at 2%). We followed the description of the Seltzer model (Seltzer *et al.* 1990) as first described in mice (Malmberg & Basbaum, 1998). Briefly, the sciatic nerve was exposed at the upper thigh level. The dorsal third to half of the sciatic nerve was tightly ligated at a site distal to nerve trifurcation with a 5-0 black nylon suture (Harvard Apparatus). In sham-operated mice, the nerve was exposed but not ligated.

Mechanical. Response to mechanical stimuli was determined using a dynamic plantar aesthesiometer (Ugo Basile, Comerio, Italy). Mice were placed on a wire mesh floor in individual compartments. A 2.5 g force was applied to the plantar surface of the hind paw and latency of paw withdrawal was recorded. Mice were tested 3 times with 3 min intervals between each test.

Heat. Response to noxious heat stimuli was determined using Hargreaves' plantar test (Ugo Basile, Comerio, Italy). Mice were placed on a glass floor in individual boxes. A radiant heat source was applied to the plantar surface of the hind paw and the latency of paw withdrawal was recorded. Mice were tested 3 times with 3 min intervals between each test.

Cold. Cold allodynia was determined using the acetone drop technique as first described by Carlton *et al.* (1994) and Choi *et al.* (1994). A 10 μl drop of acetone was applied to the plantar surface of the hind paw by forming a drop at the end of a polyethylene tube attached to a syringe. The number of flinches and licks within a 1 min period was recorded. Mice were tested 5 times with a 3 min interval between each test. Mean number of flinches and licks was calculated.

Data analysis

All data shown are mean $\pm$ S.E.M. Tests for statistical differences were carried out using either paired or unpaired Student's *t* tests or one-way ANOVA, as appropriate. The criterion for statistical significance was a value of $P < 0.05$.

Results

Role of I_h in action potential firing

We initially investigated the role of I_h in the modulation of action potential firing in response to a constant-current stimulus in neonatal rat DRG neurons. We focused on small neurons ($< 25\ \mu$m cell body diameter), of which the majority are nociceptors (Fang *et al.* 2005). We identified neurons expressing I_h by the presence of a voltage 'sag' in the membrane potential following a hyperpolarizing current step (see Fig. 1*A*). I_h was identified in 43/92 small rat neurons on this criterion, or 46.7%, in good agreement with the proportion identified as expressing I_h in voltage-clamp experiments (see below). Action potential firing was evoked using 5 s depolarizing current pulses. In all but one of the 43 small DRG neurons exhibiting I_h we observed repetitive action potential firing in response to current injection (Fig. 1*B*). The action potential frequency increased monotonically with increasing stimulus strength (Fig. 2*A*). By contrast, all large neurons ($> 35\ \mu$m, 10/10) exhibited I_h, but fired only a single action potential at all strengths of injected current.

The physiological pro-inflammatory mediator PGE_2 has been shown to sensitize nociceptive neurons by increasing their excitability (Gold *et al.* 1996; England *et al.* 1996), an effect which depends on increases in cAMP (Lopshire & Nicol, 1998). We confirmed that exposure of small I_h-expressing DRG neurons to PGE_2 ($10\ \mu$M, 4 min) enhanced their excitability, as shown by an increase in action potential frequency elicited by a current pulse (Fig. 1*B*). The increase in firing frequency was present over the whole range of test stimuli used (Fig. 2*A*), and can be attributed to a significantly increased rate of depolarization in the pacemaker region between action potentials (see Fig. 1*D*). We also observed a significant

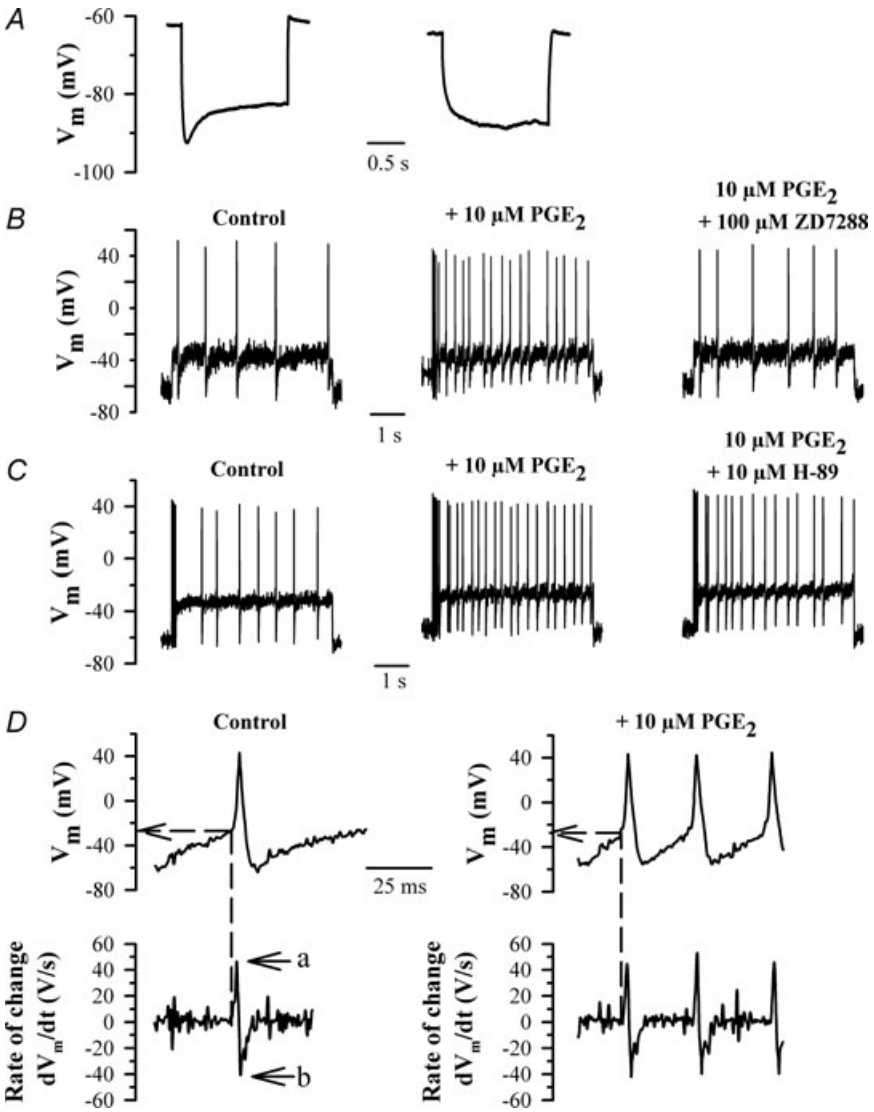

Figure 1. Enhancement by PGE_2 of action potential firing frequency in small DRG neurons
A, time-dependent rectification or voltage 'sag' of membrane potential in small ($< 25\ \mu$m diameter) rat DRG neurons. Representative traces of membrane potential following injection of a 500 pA hyperpolarizing current pulse for 2 s, showing a neuron expressing I_h (left) or not expressing I_h (right). A neuron was considered to express I_h if the amplitude of the voltage sag exceeded 10% of the initial peak voltage excursion. *B*, representative traces showing action potential firing produced by a 100 pA depolarizing current in control conditions (left), in the presence of 10 μM PGE_2 (centre), and in the presence of 10 μM PGE_2 plus 100 μM ZD7288 (right). *C*, same as *B* but in control (left), in the presence of 10 μM PGE_2 (centre) and in the presence of 10 μM PGE_2 plus 10 μM H-89 (right). Data in *B* and *C* were obtained from two different neurons. *D*, upper panels: action potentials, taken from traces in *B*, at an expanded time scale, in control conditions (left) and in the presence of 10 μM PGE_2 (right). Lower panels show the 1st derivative (dV_m/dt) of the voltage trace shown above. Arrows show maximum rate of rise ('a'), maximum rate of fall ('b').

depolarizing shift in the resting membrane potential, from -63.6 ± 2.0 to -54.7 ± 1.5 mV ($P < 0.001$, $n = 19$; Fig. 2*B*). The adenylate cyclase activator forskolin (50 μM) increased action potential frequency in a similar manner to PGE_2 (Fig. 2*A*) and also depolarized the resting membrane potential, from -64.8 ± 1.4 to -55.9 ± 1.7 mV ($P < 0.001$, $n = 11$; Fig. 2*C*). In contrast, in large neurons (> 35 μm, 10/10) application of the pro-inflammatory mediator PGE_2 or elevating cAMP levels using forskolin failed to have any effect on action potential firing, and nor was there any effect on resting membrane potential (-62.4 ± 1.7 mV in the absence of PGE_2 and -63.4 ± 1.5 mV in the presence of PGE_2, 10 μM, 4 min; $n = 10$, $P > 0.05$).

If PGE_2 acts to cause sensitization of nociceptors through a lowering of the voltage threshold or an increase in the amplitude of $Na_V1.8$ then an effect on the action potential threshold or the rate of rise of the action potential (respectively) would be expected. In a similar way, an inhibition of voltage-dependent potassium currents by

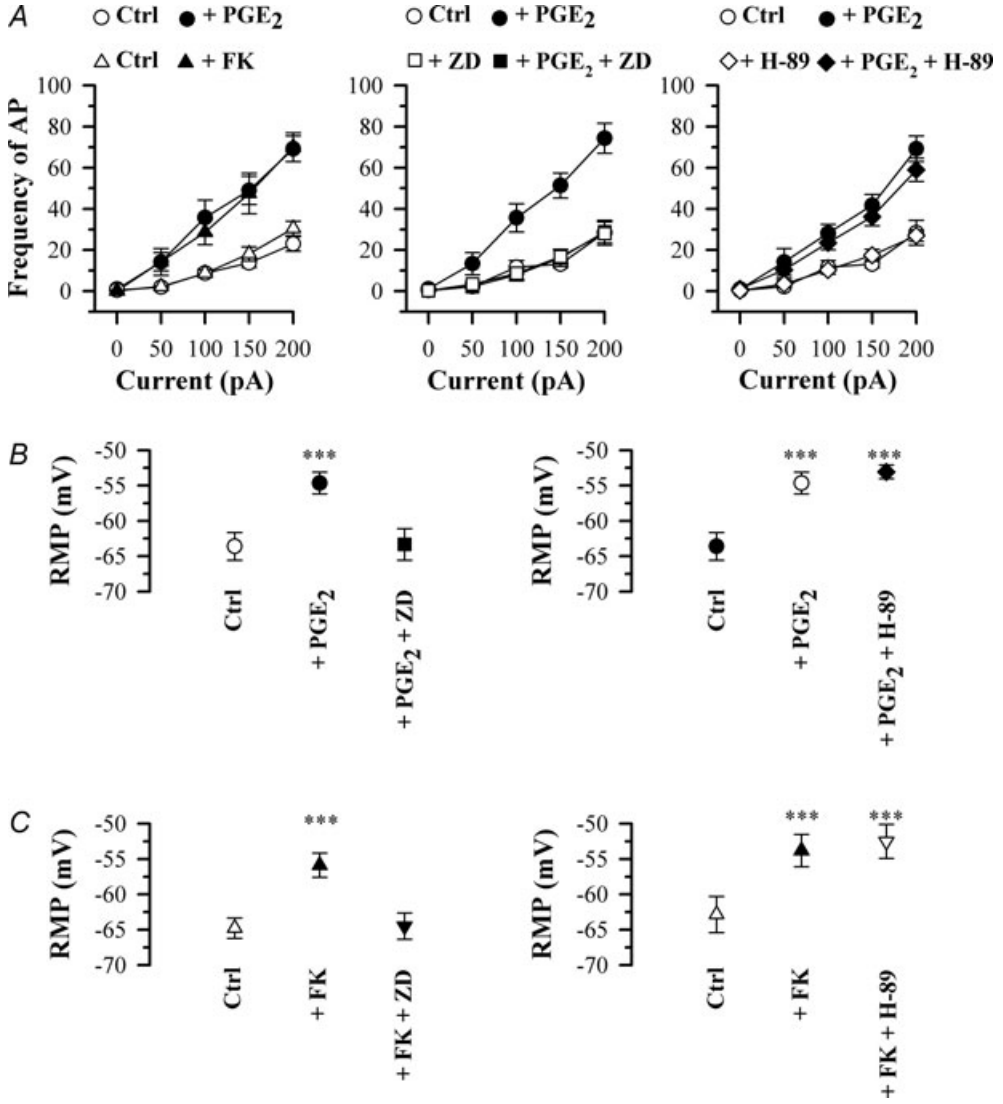

Figure 2. Effect of PGE_2, forskolin (FK), ZD7288 (ZD) and H-89 on action potential firing in small (< 25 μm) rat DRG neurons

A, frequency of AP firing in response to increasing injected current strength in the following conditions: left panel, control conditions (○) and in 10 μM PGE_2 (●, $n = 19$), or (in a separate series of experiments) in control (△) and in 50 μM forskolin (FK) (▲, $n = 11$); centre panel, control (○), 10 μM PGE_2 (●), 100 μM ZD7288 (□), 10 μM PGE_2 and 100 μM ZD7288 (■, $n = 13$); right panel, control (○), 10 μM PGE_2 (●),10 μM H-89 (◇), 10 μM PGE_2 and 10 μM H-89 (◆, $n = 6$). *B*, effect on mean resting membrane potential (RMP) of 10 μM PGE_2 alone and with 100 μM ZD7288 (left panels, $n = 6$) and alone and with 10 μM H-89 (right panels, $n = 5$). *C*, similar series of experiments in which 50 μM forskolin (FK) was used in place of PGE_2 (left panels, $n = 6$; right panels, $n = 5$). Significance levels compared to control: ***$P < 0.001$.

PGE_2 (Nicol *et al.* 1997) should cause a decrease in the rate of fall of the repolarization phase of the action potential. We estimated these parameters by calculating the first derivative of membrane potential, dV_m/dt (Fig. 1*D*). The value of dV_m/dt is positive during the interval between action potentials, and abruptly increases as the action potential upstroke begins (see Fig. 1*D*). We estimated the action potential threshold from the membrane potential at the moment when dV_m/dt attains its minimum value immediately before the action potential upstroke (dashed lines in Fig. 1*D*). Prior to exposure to PGE_2 the action potential threshold was -34.7 ± 1.4 mV, while after PGE_2 application it was -33.8 ± 1.5 mV ($P > 0.05$, difference not significant, $n = 19$; Table 1). Forskolin also failed to have any significant effect on action potential threshold (Table 1). Furthermore, neither the maximum rate of rise nor the maximum rate of fall of the action potential ('a' and 'b' in Fig. 1*D*) was significantly affected by either PGE_2 or forskolin (Table 1). These results argue against a major effect of increases in cAMP on either the voltage-dependent Na^+ or K^+ currents.

Figure 1*B* shows that the effect of PGE_2 on neuronal excitability was completely reversed by the specific I_h blocker ZD7288 (Harris & Constanti, 1995). Over the whole range of currents tested, ZD7288 reversed the enhancement in action potential frequency to a level not significantly different from that before application of PGE_2 (Fig. 2*A*). Furthermore, the resting membrane potential was hyperpolarized by ZD7288 from -54.7 ± 1.5 to -64.5 ± 1.9 mV ($n = 13$), the latter value being not significantly different from the resting potential before application of PGE_2 (Fig. 2*B*). ZD7288 also caused a similar inhibition of the enhanced excitability observed when adenylate cyclase was activated directly with forskolin (not shown), and also reversed the depolarization of resting membrane potential seen following application of forskolin (Fig. 2*C*).

We conducted experiments in the presence of a PKA inhibitor, H-89 (10 μM), to investigate a possible contribution of signalling via PKA to the enhanced action potential firing. As shown in Figs 1*C* and 2*A*, H-89 had little effect on the enhanced excitability following application of PGE_2. The resting membrane potential remained depolarized (-52.5 ± 2.4 mV, not significantly different from value of -53.7 ± 1.2 mV in PGE_2 alone, $n = 6$, Fig. 2*B*) while the action potential threshold remained unchanged, as did the maximum rate of rise and maximum rate of fall of the action potential (Table 1). H-89 also had little effect on the membrane depolarization caused by forskolin (Fig. 2*C*). From these experiments and those above we conclude that the major action of PGE_2 in enhancing action potential frequency occurs directly through increases in cAMP, and that any effect caused by PKA-dependent phosphorylation of downstream ion channel targets is small.

Table 1. Effect of PGE_2 (10 μM), forskolin (50 μM), ZD7288 (100 μM) and H-89 (10 μM) on parameters of action potentials in small rat DRG neurons (see Figs 1 and 2)

Condition	AP threshold (mV)	Rate of rise dV_m/dt ($V\,s^{-1}$)	Rate of fall dV_m/dt ($V\,s^{-1}$)
Ctrl	-34.7 ± 1.4	41.4 ± 0.7	-41.2 ± 2.0
+ PGE_2	-33.8 ± 1.5	41.9 ± 2.5	-40.3 ± 0.6
+ PGE_2 + ZD7288	-34.1 ± 1.3	41.9 ± 0.9	-40.6 ± 1.4
+ PGE_2 + H-89	-34.1 ± 0.7	41.1 ± 1.2	-41.2 ± 0.7
Ctrl	-33.9 ± 0.8	42.2 ± 1.4	-42.4 ± 0.9
+ FK	-33.3 ± 0.5	43.0 ± 1.8	-41.3 ± 1.3
+ FK + ZD7288	-33.8 ± 0.9	42.2 ± 1.4	-41.8 ± 0.8
+ FK + H-89	-34.5 ± 1.2	41.9 ± 2.7	-40.6 ± 1.4

None of the three parameters in the table was significantly affected by any of these treatments. Number of neurons $n = 5$–6 for all measurements.

Dependence of I_h on neuronal size

Sensory afferent nerve fibres are classified into three main categories: large-diameter, fast-conducting myelinated Aβ-fibres, which serve a variety of mainly non-nociceptive functions; smaller and slower myelinated Aδ-fibres, some of which are nociceptive and others non-nociceptive; and the smallest and slowest unmyelinated C-fibres, the majority of which are nociceptors (Lawson, 2002). A correlation exists between cell body diameter and conduction velocity of the afferent fibre in adult rat, with Aβ-fibres having a mean cell body diameter of 38 μm, Aδ-fibres 30 μm and C-fibres 24 μm (Harper & Lawson, 1985). Cell body sizes are smaller in the neonatal rats used in the present study, so in order to classify rat neurons approximately into the three main functional classes we employed a classification as follows: large (> 35 μm), medium (25–35 μm) and small (< 25 μm).

I_h in DRG neurons was activated by imposing membrane potential steps in whole-cell voltage-clamp mode in 10 mV increments from a holding potential of -60 mV (Fig. 3*A* and *B*). The steady-state voltage dependence of I_h activation was determined from the initial amplitudes of tail currents at a final step potential of -160 mV. Activation curves were fitted with a Boltzmann equation (see Methods) to determine the midpoint of voltage activation, $V_{1/2}$, and the slope factor, k (Fig. 3*C*). Time constants of current activation were determined by fitting double-exponential functions (Fig. 3*D*); note that two time constants are required to fit the activation of even homomeric HCN subunits in expression systems (Santoro *et al.* 2000). The example shown in Fig. 3 is typical of a large

rat DRG neuron (> 35 μm diameter); the characteristics of I_h in other size classes of neurons are different (see below).

I_h was considered to be present in a DRG neuron if the time-dependent inward current activated by a voltage step to −160 mV (see Fig. 3*B*) was greater than 50 pA. On this criterion I_h was observed in 37 out of 87 small neurons (42.5%), 68 out of 101 medium neurons (67.3%) and 50 out of 50 large neurons (100%) as shown in Fig. 4*A*, in line with earlier reports (Scroggs *et al.* 1994; Yagi & Sumino, 1998). The proportion of small neurons expressing I_h was also similar on this criterion to that obtained with current injection (46.7%, see above). Fifteen out of 20 small neurons expressing I_h also expressed TRPV1 and/or P2X3, as shown by the presence of inward currents activated by capsaicin or the P2X3 receptor agonist α,β-methyl ATP (see example traces in Fig. 5), and therefore have the properties of nociceptors.

There was a marked difference in the activation time constants of I_h among the different classes of rat DRG neurons (Fig. 4*B*). The mean value of τ_f, the fast-activation time constant that accounts for 75–85% of the I_h current amplitude in all neurons, was 154.8 ± 17.1 ms ($n = 50$) in large neurons and 942.6 ± 80.4 ms ($n = 37$, $P < 0.001$) in small neurons at −90 mV, a more than sixfold difference (see Fig. 4*B*). In medium rat neurons two kinetically distinct populations of I_h were present: a fast-activating population with time constants similar to those obtained in large neurons, and a second population with slower activation of I_h (Fig. 4*B*). There is little overlap in the values of time constants between these two populations (see Fig. 4*B*) and we therefore termed them 'medium fast' ($\tau_f < 400$ ms) and 'medium slow' ($\tau_f > 400$ ms). No significant difference in mean cell body diameter was observed between medium fast and medium slow neurons (32.5 ± 1.3 and 31.0 ± 1.5 μm, respectively). I_h in the medium slow population was, however, significantly faster-activating than that in small neurons (Fig. 4*B*).

A further important point to note is that a minor population of small neurons had a fast-activating I_h indistinguishable from that seen in large neurons (Fig. 4*B*). This population comprised 9% of the small neurons and 2% of the total, and was readily distinguishable from the remaining 91% of small neurons, which express an I_h which activates on average 6 times more slowly (see Fig. 4*B*). Small neurons with fast I_h may correspond to cold-sensitive neurons, which form less than 5% of the DRG neuronal population (S. Mak, unpublished observations) and have a fast-activating I_h (Viana *et al.* 2002). We therefore tested for expression of the cold-sensitive ion channel TRPM8 by applying menthol, which is a specific activator of TRPM8 (McKemy *et al.* 2002). Figure 5 shows that small neurons with fast I_h were sensitive to menthol. These cells did not respond to the TRPV1 agonist capsaicin or the P2X3 agonist α,β-methyl ATP. The time constant of the fast-activating I_h in these menthol-sensitive small neurons was indistinguishable from that in large neurons but was highly significantly different from that in the non-menthol-sensitive small neurons ($P < 0.001$, Fig. 5*D*). Small neurons responding

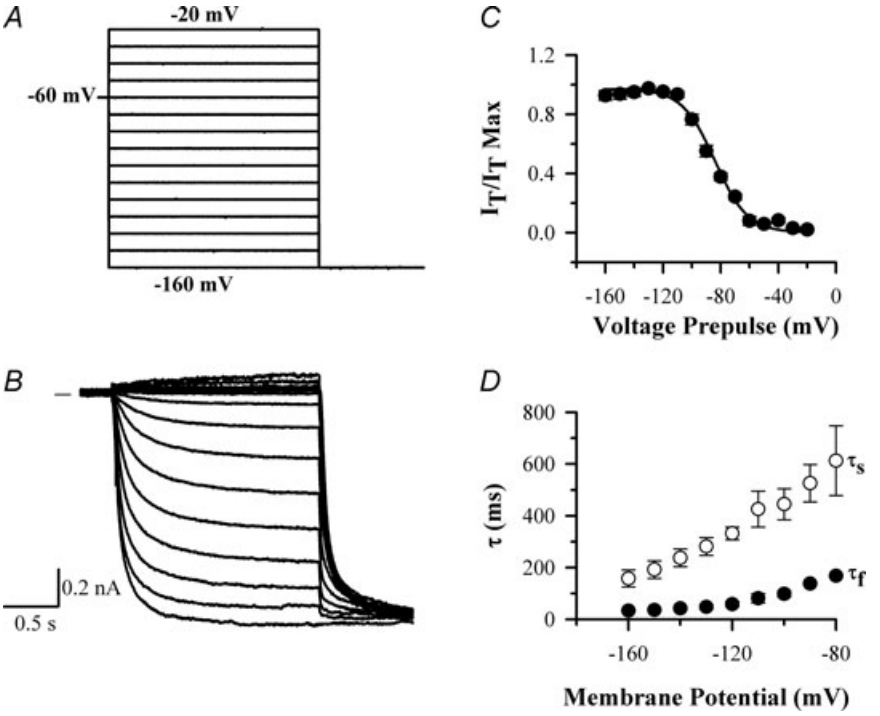

Figure 3. Voltage-clamp traces of I_h recorded from a large neuron using the caesium-subtraction technique
A, voltage protocol; I_h was activated from a holding potential of −60 mV in 2 s pulses from −20 mV to −160 mV in 10 mV increments, followed by a final step to −160 mV. *B*, Cs-subtracted traces, following subtraction of current traces in which I_h had been completely inhibited by application of 5 mM CsCl. Zero current level shown by horizontal line in this and other traces. *C*, activation of I_h as a function of membrane voltage, obtained from the magnitude of the I_h tail current at the start of the −160 mV test potential. Trace fitted to points with parameters $V_{1/2} = -81.4 \pm 1.3$ mV, slope factor $s = 11.6 \pm 1.0$ mV. *D*, time constants as a function of membrane voltage. I_h current traces were fitted with sum of two exponentials as described in Methods to obtain a fast (τ_f, ●) and slow time constant (τ_s, ○).

to capsaicin or to α,β-methyl ATP, on the other hand, had a slowly activating I_h indistinguishable from that of the overall small neuron population (Fig. 5*D*).

In summary, we identify four distinct neuronal populations, based on the time constants of activation of I_h and cell diameter: (1) large and medium fast cells, both of which express a similar fast-activating I_h; (2) medium slow cells, which express an I_h which activates with an intermediate time constant; (3) the majority of small cells, which express a slowly activating I_h; and (4) a minor population of small cells, which express TRPM8 and a fast-activating I_h.

Sensitivity to cAMP as a function of neuronal size

The activation of HCN2 and HCN4 as a function of membrane voltage is markedly sensitive to intracellular cAMP, while HCN1 and HCN3 are relatively insensitive. To investigate further the possible molecular basis of native I_h in sensory neurons we elevated intracellular levels of cAMP in three separate ways: by activating adenylate cyclase with forskolin; by applying PGE_2; or by applying cAMP directly via the patch pipette.

Extracellular application of 50 μM forskolin for 4 min to large rat neurons had no detectable effect on the voltage sensitivity or the time constant of activation of I_h. $V_{1/2}$ was -81.6 ± 1.6 mV in the absence and -81.4 ± 2.1 mV in the presence of forskolin ($n = 10$, $P > 0.05$), and there was no change in the voltage dependence of τ_f (Fig. 6*A*). There was also no effect on I_h in large neurons following application of 10 μM PGE_2 nor when 50 μM cAMP was present in the patch pipette, as determined by calculating $\Delta V_{1/2}$ ($+0.7 \pm 0.9$ mV, $n = 10$, and $+0.2 \pm 1.2$ mV, $n = 12$, respectively, neither significant). A similar lack of effect of forskolin, PGE_2 or intracellular cAMP on the activation of I_h was also observed in medium fast neurons (Fig. 6*B* and Table 2).

In contrast, most small and all medium slow neurons responded with a depolarizing shift in $V_{1/2}$ in the presence of 50 μM forskolin, from -86.3 ± 1.6 to -72.5 ± 1.8 mV ($n = 11$) and -85.9 ± 1.0 to -71.5 ± 1.7 mV ($n = 12$), respectively (Fig. 6*C* and *D*, and Table 2). There was a corresponding shift in the dependence of the time constants of activation of I_h on membrane voltage in these two classes of neurons (Fig. 6*C* and *D*). Elevations in cAMP caused by either exogenous application of PGE_2

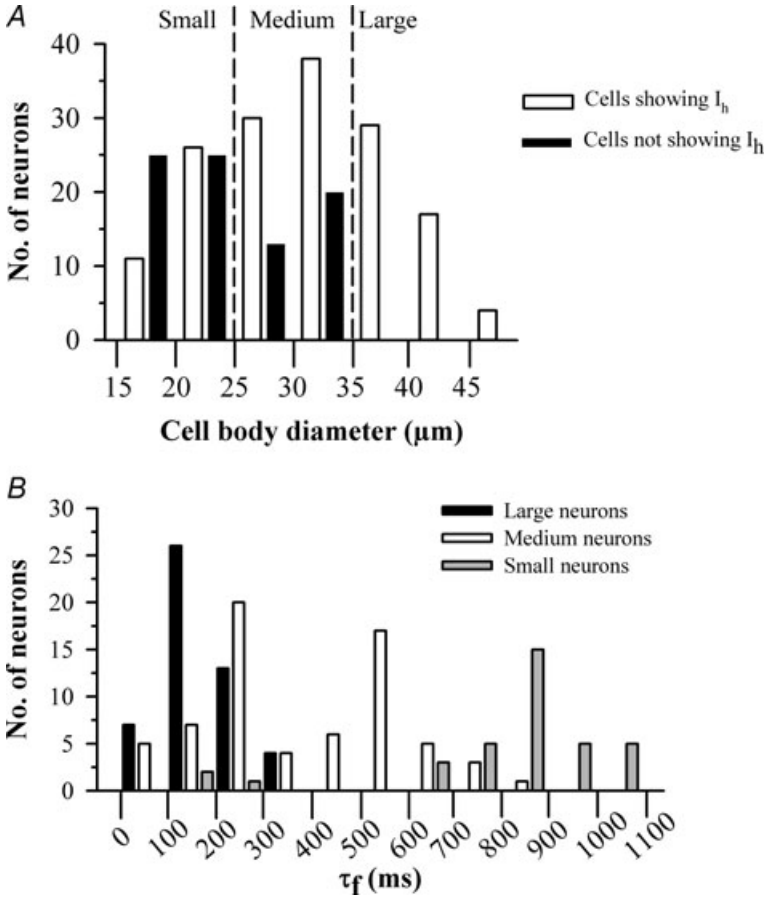

Figure 4. Properties of I_h in 3 size classes of rat DRG neurons
A, histogram showing numbers of neurons which show I_h (amplitude of I_h at -60 mV > 50 pA, open bars) or do not show I_h (amplitude of I_h at -160 mV < 50 pA, black bars) in relation to cell body diameter.
B, histogram showing τ_f values, obtained at a membrane potential of -90 mV, in the three classes of rat neurons: large (black bars, > 35 μm); medium (open bars, 25–35 μm); and small (grey bars, < 25 μm).

or by including cAMP in the patch pipette, also brought about quantitatively similar depolarizing shifts in the I_h voltage-activation curve in both populations of neurons (not shown). Small neurons with fast-activating I_h, by contrast, were insensitive to elevation of cAMP, with $\Delta V_{1/2} = 0.5 \pm 0.3$ mV in the presence of 50 μM forskolin ($n = 3$). Results for the effects of forskolin on $V_{1/2}$ in the four major classes of neurons are summarized in Fig. 6*E* and Table 2.

The results presented in Figs 4–6 show that large and medium-fast neurons, and a small population of TRPM8-expressing small neurons, express a fast-activating, cAMP-insensitive I_h, consistent with the expression of HCN1. Medium slow and small neurons express two variants of slower-activating I_h, both of which are sensitive to cAMP and are therefore consistent with expression of HCN2 and/or HCN4. We further investigated the HCN isoform distribution in DRG neurons by constructing a HCN1$^{-/-}$ mouse.

I_h in mouse HCN1$^{+/+}$ and HCN1$^{-/-}$ DRG neurons

Adult mouse DRG neurons are smaller than rat, so a revision of the size classes was required for mouse neurons. The mean diameter of cell bodies subtending fast-conducting Aβ-fibres is 31 μm and of unmyelinated slow-conducting C-fibres is 14 μm (Yoshida & Matsuda, 1979). In a more recent study neurons binding the plant lectin IB4, which are a subpopulation of unmyelinated C-fibres (Snider & McMahon, 1998), had a mean diameter ~17 μm (Stucky & Lewin, 1999). We therefore classified mouse neurons into three size classes: large (> 30 μm), medium (20–30 μm) and small (< 20 μm).

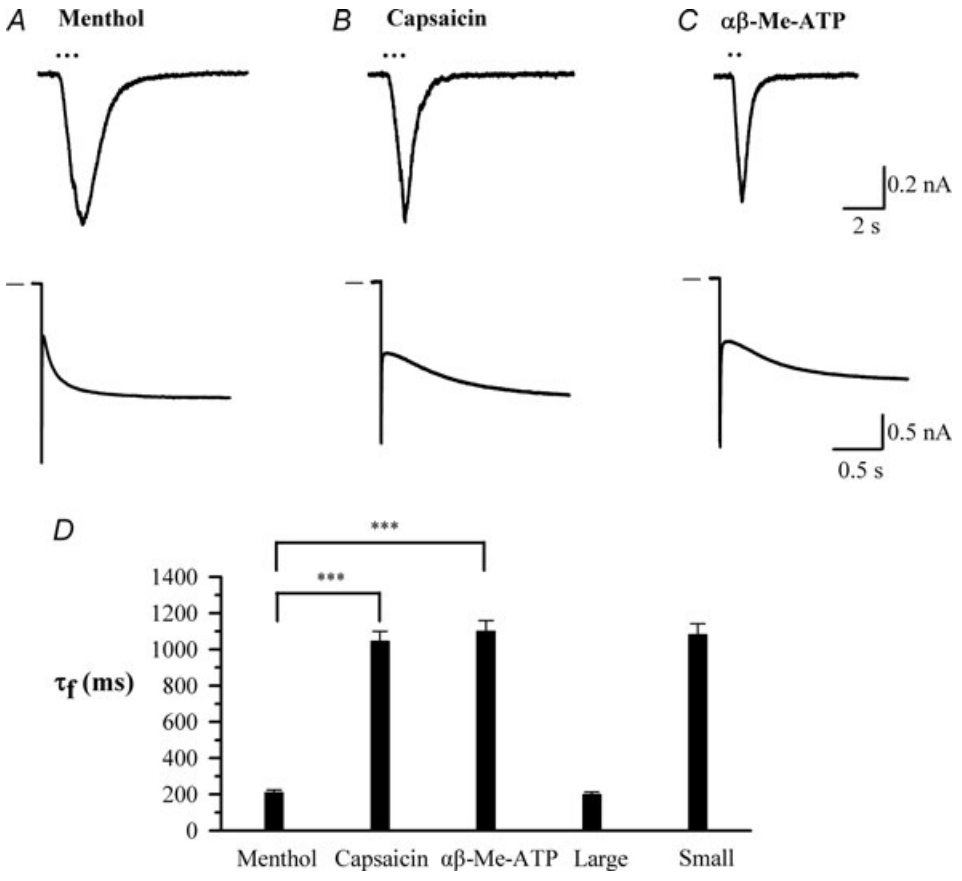

Figure 5. A subpopulation of small rat DRG neurons expresses TRPM8 and has fast-activating I_h
A–C, sample inward currents activated by a 1 s exposure to menthol (50 μM), capsaicin (1 μM) and α,β-methyl ATP ($\alpha\beta$-Me-ATP; 10 μM) in three different small neurons (< 25 μm); and I_h activated in the same neurons by a voltage step from −60 mV to −90 mV. The cell responding to menthol did not respond to either capsaicin or $\alpha\beta$-Me-ATP. *D*, time constants of the fast component of I_h in each class of neuron compared with the overall time constants for large (> 35 μm) and small (< 25 μm) neurons. ***$P < 0.001$ for the comparisons indicated. Note that data in this figure were obtained without the use of the Cs-subtraction technique, and values of time constants are therefore not directly comparable with those given in other figures which were all obtained using Cs-subtraction.

In mouse HCN1$^{+/+}$ neurons I_h was present in 26/26 (100%) of large neurons, 47/57 (82.4%) of medium neurons and 30/68 (44.1%) of small neurons, proportions which are identical within experimental error to the corresponding data obtained for rat neurons. Values of $V_{1/2}$ were ~5 mV more negative than in rat (Table 2). Values and distributions of τ_f in the three size classes in HCN1$^{+/+}$ mice were very similar to those for rat (see Fig. 7*E* and Table 2). A fast-activating I_h was found in large HCN1$^{+/+}$ DRG neurons and in

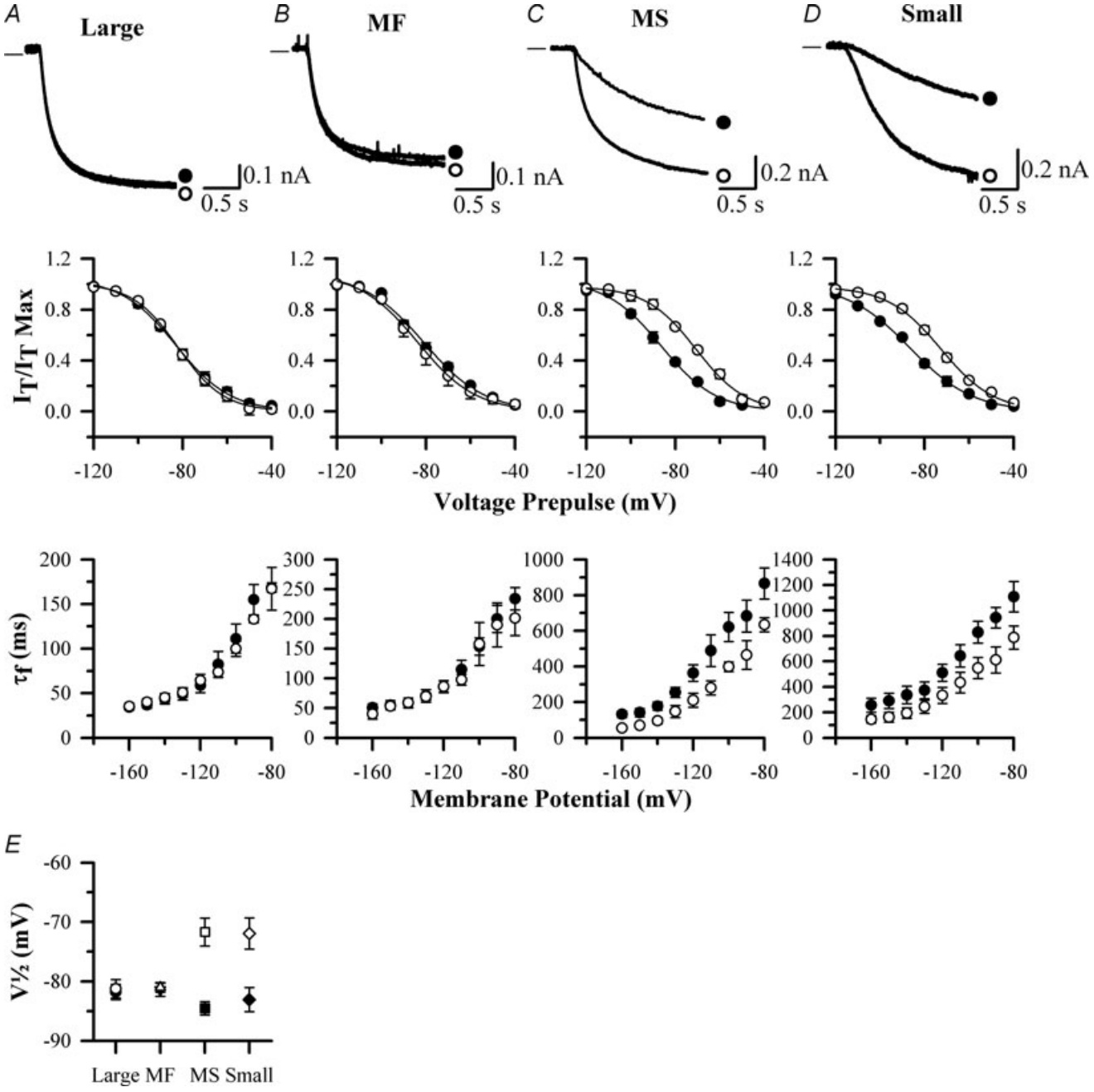

Figure 6. Effect of elevation of cAMP on properties of I_h in rat DRG neurons of different sizes
A, *B*, *C* and *D* show properties of activation of I_h in rat large (*A*), medium fast (MF, *B*), medium slow (MS, *C*) and small DRG neurons (*D*). Upper panels show representative current traces in response to a voltage pulse from −60 mV to −90 mV in the absence (●) and presence (○) of 50 μM FK. Middle panels show steady-state activation curves of I_h as a function of membrane voltage over the range −120 mV to −40 mV in the absence (●) and presence (○) of 50 μM FK. Lower panels show τ_f in absence (●) and presence (○) of 50 μM FK. *E*, effect of 50 μM FK on values of $V_{1/2}$ in the four populations of rat DRG neurons shown in *A*–*D*. Absence and presence of 50 μM FK is shown by filled or open symbols, respectively. Experiments repeated n = 10–15 times in each neuronal population.

Table 2. Comparison of parameters of activation of I_h in the four main classes of rat and mouse HCN1$^{+/+}$ DRG neurons

	Large		Medium fast		Medium slow		Small	
	Rat	Mouse	Rat	Mouse	Rat	Mouse	Rat	Mouse
Size classes (μm)	> 35	> 30	25–35	20–30	25–35	20–30	< 25	< 20
$V_{1/2}$ (mV)	-81.6 ± 1.6	-84.3 ± 2.4	-81.1 ± 1.6	-86.7 ± 2.4	-85.9 ± 1.0	-91.4 ± 1.9	-86.3 ± 1.6	-88.3 ± 1.4
τ_f (ms, at -90 mV)	155 ± 17	101 ± 28	200 ± 56	178 ± 38	622 ± 90	652 ± 68	943 ± 80	830 ± 87
τ_s (ms, at -90 mV)	526 ± 72	443 ± 39	929 ± 109	727 ± 71	1378 ± 128	1352 ± 125	2146 ± 235	1616 ± 107
$\Delta V_{1/2}$ (mV) FK	0.2 ± 0.5	1.3 ± 0.9	1.9 ± 0.6	0.9 ± 0.5	14.4 ± 0.7	13.2 ± 1.9	13.8 ± 0.4	16.7 ± 0.5

All data from Cs-subtracted current traces. The value of $V_{1/2}$ was almost unaffected by forskolin (FK, 50 μM) in large and medium fast neurons, but was shifted in the positive direction by $\sim$14 mV in both medium slow and small neurons (see also Fig. 6*E*). Similar results were also obtained in rat neurons with exposure to PGE_2 (10 μM) and with cAMP (50 μM) incorporated into the patch-clamp pipette. Number of neurons $n = 10$–15 for each measurement.

a subpopulation of medium HCN1$^{+/+}$ neurons (Fig. 7*A* and *B*), which we label medium fast by analogy with rat neurons. This population was broadly similar in its properties to the corresponding population in rat, though a small number of neurons had significantly longer time constants than was found in rat (compare black bars in Figs 4*B* and 7*E*). Application of forskolin (50 μM) to large and medium-fast neurons (including the small number with longer time constants than found in rat) had no significant effect on $V_{1/2}$ (Table 2) or activation time constant (data not shown). A second subpopulation of medium-sized HCN1$^{+/+}$ neurons had intermediate activation time constants, forming a distinct group from the medium-fast neurons. This population was similar to the rat medium-slow neuronal population (Fig. 7*E*). The majority of small neurons had an even slower I_h (grey bars in Fig. 7*E*). Application of 50 μM forskolin caused 13–14 mV depolarizing shifts in the values of $V_{1/2}$ (Table 2) and in the voltage dependence of the activation time constant (not shown) in both medium-slow and small mouse neurons. As in rat, a small subpopulation of small neurons had fast time constants (Fig. 7*E*), and the $V_{1/2}$ of I_h in these neurons was insensitive to forskolin ($\Delta V_{1/2} = 0.4 \pm 0.2$ mV, $n = 3$). These results are closely similar to the corresponding results for neonatal rat neurons, when the size difference between neonatal rat and adult mouse neurons is taken into account.

We next examined the effect of genetic deletion of HCN1. In 9 out of 12 large DRG neurons from HCN1$^{-/-}$ mice no I_h could be detected (Fig. 7*A*, lower panel). This is in contrast to the 26 out of 26 HCN1$^{+/+}$ large DRG neurons that showed a fast-activating I_h using the same voltage pulse protocol. The absence of I_h in most large HCN1$^{-/-}$ neurons is also reflected in an absence of fast τ_f values in this group of neurons (Fig. 7*F*). These results show that HCN1 is the only isoform contributing to the fast I_h present in the majority of large DRG neurons. In the three large neurons in which I_h was present, it was slow activating, with a mean τ_f of 474.5 ± 169.8 ms ($n = 3$), and was cAMP insensitive. A current with these properties was not recorded in any rat or HCN1$^{+/+}$ mouse neuron. A likely explanation is that this current reflects expression of HCN3, which activates slowly and is insensitive to cAMP (Stieber *et al.* 2005), and that the presence of HCN3 is masked in HCN1$^{+/+}$ neurons by coexpression of the fast-activating HCN1 (discussed further below).

In medium HCN1$^{-/-}$ neurons two main populations were present: one in which no I_h could be detected (10 out of 39 medium neurons, see Fig. 7*B* lower panel), and a second, and more prevalent population (29 out of 39 medium neurons, see Fig. 7*C*) in which a slower I_h was seen, with τ_f at -90 mV of 534.5 ± 109.8 ms, a value similar to that of the medium slow neurons in HCN1$^{+/+}$ mice (Fig. 7*F*). Unlike the mouse HCN1$^{+/+}$ or rat medium slow neuron population, however, this was not a single population because application of 50 μM forskolin produced two distinct results. In 10 out of 29 neurons (medium slow 1), forskolin failed to have any effect on activation of I_h (Fig. 8*A*), a result in contrast to the rat or mouse HCN1$^{+/+}$ medium slow neurons, which all responded to forskolin with a shift in $V_{1/2}$. The insensitivity to cAMP and the slow activation of I_h in these neurons suggests the presence of HCN3, the activity of which is not modulated by cAMP (Stieber *et al.* 2005). The fact that no analogous population was present in HCN1$^{+/+}$ neurons suggests that HCN3 normally forms heteromers with HCN1, and that these heteromers activate rapidly and therefore contribute to the 'medium fast' neuronal population. In the remaining medium slow neurons (19 out of 29, medium slow 2) forskolin caused I_h to activate faster and shifted $V_{1/2}$ from -85.3 ± 1.7 to -72.0 ± 1.2 mV (Fig. 8*B*), a result indistinguishable from the behaviour of mouse HCN1$^{+/+}$ or rat medium slow neurons.

In small neurons I_h was unaffected by the deletion of HCN1 (Fig. 7*D*). The proportion of neurons expressing I_h (12/26 or 46.2%) was similar to that in mouse HCN1$^{+/+}$ and rat small neurons. The values of τ_f and $V_{1/2}$ in mouse HCN1$^{-/-}$ small neurons were similar to those obtained in

HCN1$^{+/+}$ neurons. Application of forskolin to HCN1$^{-/-}$ small neurons caused a shift in $V_{1/2}$ from -87.4 ± 1.5 to -69.6 ± 1.1 mV ($n = 27$, see Fig. 8*C*) and a corresponding shift in the voltage dependence of the values of τ_f (data not shown). These values are indistinguishable from those obtained in small mouse HCN1$^{+/+}$ and rat neurons (Table 2), with the exception that no small neurons with fast-activating I_h were found.

In summary, these results show that the majority of large neurons, and some medium fast neurons, express only HCN1, and that therefore on deletion of HCN1 no I_h remains. The remaining large and medium-fast neurons are likely to coexpress HCN1 and HCN3, so that following deletion of HCN1 only HCN3 remains, generating a slowly activating, cAMP-insensitive I_h. Medium slow neurons and the large majority of small neurons do not express HCN1, so their properties are unaltered by deletion of HCN1. However, the subpopulation of small neurons with a fast-activating, cAMP-insensitive I_h, which therefore probably expressed HCN1, was absent in HCN1$^{-/-}$ mice.

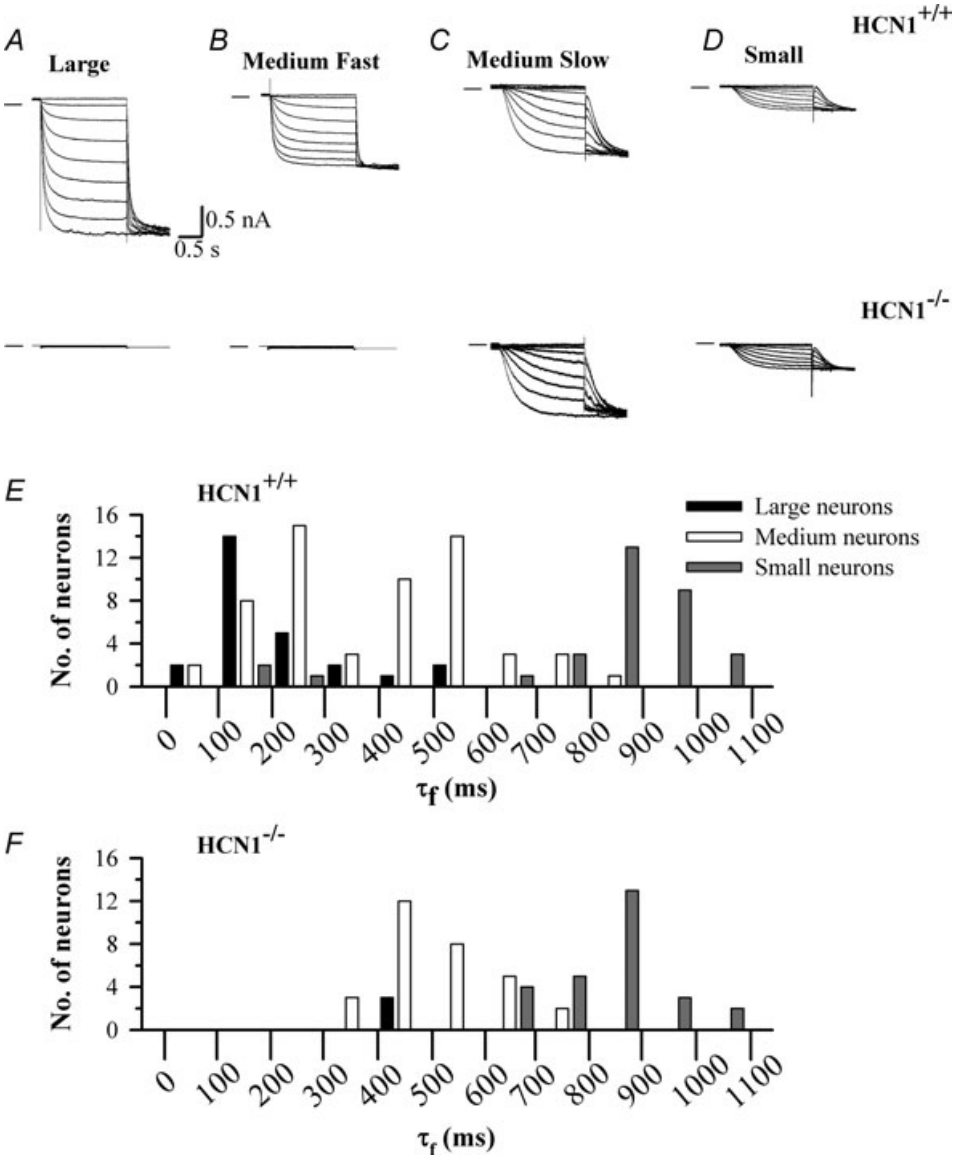

Figure 7. Recordings of I_h from mouse HCN1$^{+/+}$ and HCN1$^{-/-}$ DRG neurons
A, *B*, *C* and *D* show representative recordings of I_h in large (*A*), medium fast (*B*), medium slow (*C*) and small DRG neurons (*D*), from HCN1$^{+/+}$ (upper panel) and HCN1$^{-/-}$ mice (lower panel). I_h was activated from a holding potential of −60 mV in 10 mV steps followed by a final step to −140 mV. *E*, histogram showing τ_f values derived at a membrane potential of −90 mV in the three classes of mouse HCN1$^{+/+}$ neurons. *F*, similar histogram for HCN1$^{-/-}$ neurons.

The menthol sensitivity of these neurons was not tested but it seems likely that this population corresponds to the small TRPM8-expressing neurons identified in rat.

Role of HCN1 in inflammatory and neuropathic pain

We assessed the *in vivo* role of HCN1 channels in hyperalgesia and neuropathic pain by comparing the responses in $HCN1^{+/+}$ and $HCN1^{-/-}$ littermates to mechanical and thermal stimuli in both inflammatory and neuropathic pain models. Inflammatory pain was induced by injecting the pro-inflammatory mediator PGE_2 into the hind paw. Figure 9*A* shows a reduction in paw withdrawal latency in response to mechanical and heat stimuli following intradermal injection of 0.75 nmol PGE_2. The reduction was present for 0.5, 1 and 2 h following PGE_2 injection and returned to baseline after 24 h. No significant difference between $HCN1^{+/+}$ and $HCN1^{-/-}$ mice was seen in paw withdrawal latency in response to a mechanical stimulus. Heat hyperalgesia was also little affected by deletion of HCN1 (Fig. 9*A*).

We implemented the partial sciatic nerve ligation model (PNL, Seltzer *et al.* 1990; Malmberg & Basbaum, 1998) in order to study a possible role of HCN1 in neuropathic pain. PNL caused the development of mechanical hyperalgesia and cold allodynia in both $HCN1^{+/+}$ and $HCN1^{-/-}$ mice (Fig. 9*B*). These effects were observed from the first test point on day 4 and remained unchanged for the remainder of the study (14 days). Mechanical hyperalgesia was similar between $HCN1^{+/+}$ and $HCN1^{-/-}$ mice following PNL; a significant difference seen at 7 days was not confirmed at other time points (Fig. 9*B*, upper panel). There was, however, a sustained and highly significant reduction in cold allodynia in $HCN1^{-/-}$ mice following PNL (Fig. 9*B*, lower panel). Cold allodynia, measured from the number of flinches or licks following application of the cooling drop of acetone, was more than halved by deletion of HCN1 and the effect persisted unchanged throughout the course of the experiment.

Discussion

The role of I_h in modulation of action potential firing in sensory neurons has received little attention, but our results show that it is a major determinant of action potential firing frequency in about half of small nociceptive neurons. An increase of intracellular cAMP levels produced two major effects, both consistent with enhanced activation of I_h: an increase in the rate of depolarization of the pacemaker potential region between action potentials, and a depolarization of the resting membrane potential. Both effects were completely reversed by the specific I_h blocker ZD7288, and neither was affected by blockade of PKA.

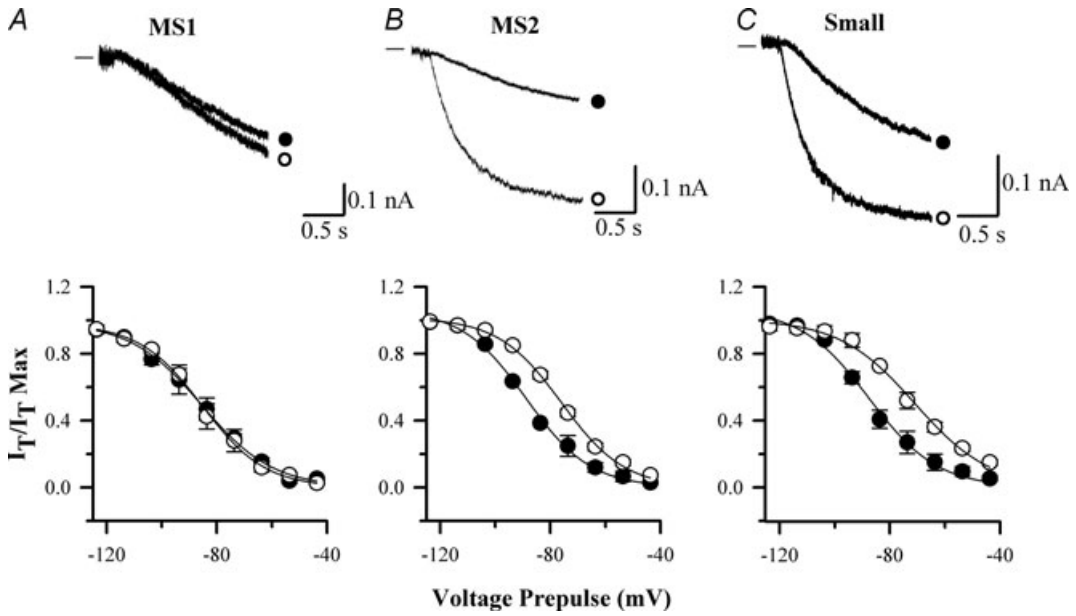

Figure 8. cAMP sensitivity of I_h in mouse $HCN1^{-/-}$ neurons
A, *B* and *C* are representative recordings of I_h activation in medium slow 1 (*A*, MS1), medium slow 2 (*B*, MS2) and small DRG neurons (*C*) from $HCN1^{-/-}$ mice. Upper panel: I_h was activated by a voltage pulse from −60 mV to −90 mV in the absence (●) and presence (○) of 50 μM FK. Lower panel: activation curves of I_h as a function of membrane voltage in the absence (●) and presence (○) of 50 μM FK. Time constants in the MS1 and MS2 classes are similar but MS1 neurons are cAMP insensitive. Experiments repeated $n = 10$–15 times in each neuronal population.

Voltage-clamp experiments showed that elevating cAMP levels shifted the voltage-activation curve of I_h in small nociceptive neurons, but not in large neurons, to more depolarized potentials. This shift has the effect both of increasing the amplitude of inward current carried by I_h and of increasing its rate of activation. A third important effect is the steady depolarization of the resting membrane potential caused by tonic activation of I_h, which is equivalent to a constant current injection at the resting potential.

Modulation of voltage-dependent sodium or potassium channels has to date been considered the most probable explanation for the enhanced firing of nociceptors in the presence of pro-inflammatory mediators such as PGE_2. Modulation of $Na_V1.8$ sodium channels via the cAMP/PKA pathway has been proposed to lower the activation threshold and increase the amplitude of the voltage-activated Na^+ current in nociceptive neurons (Gold *et al.* 1996; England *et al.* 1996), but no effect of PGE_2 or forskolin on action potential threshold or rate of rise was observed in the present experiments. There was also no effect on the rate of repolarization following an action potential, suggesting that suppression of voltage-dependent potassium conductance (Nicol *et al.* 1997) is unlikely to play an important role. The enhanced excitability was instead completely suppressed by ZD7288, a specific inhibitor of I_h, but was unaffected by H-89, an inhibitor of PKA. These experiments show that I_h is a major determinant of the enhanced nociceptor excitability caused by exposure to pro-inflammatory mediators.

HCN isoforms responsible for I_h

Large DRG neurons express a fast-activating I_h (Chaplan *et al.* 2003; Yao *et al.* 2003; Doan *et al.* 2004; Tu *et al.* 2004). The values of τ_f at -90 mV obtained in the present study in large neurons, 155 ± 17 ms, or in the medium fast class of neurons, 200 ± 56 ms, are not significantly different and are similar to the values obtained for the cloned HCN1 channel (Santoro *et al.* 2000; Chen *et al.* 2001). The lack of effect of cAMP on the voltage dependence of I_h in large and medium-fast neurons is also consistent with expression of HCN1. These findings suggest a major involvement of HCN1 in large and medium-fast neurons, but they do not exclude the possible presence of coexpressed HCN3. The absence of cAMP sensitivity makes an involvement of HCN2 or HCN4 unlikely. These results were supported by the absence of I_h in most large $HCN1^{-/-}$ neurons (Fig. 7), and by *in situ* hybridization and immunohistochemistry data (Moosmang *et al.* 2001; Chaplan *et al.* 2003) showing high levels of HCN1 mRNA and protein expression in large and medium DRG neurons. A slower, cAMP-insensitive I_h was found in some $HCN1^{-/-}$ large and medium-sized neurons; no current with these properties was observed in any mouse $HCN1^{+/+}$ or rat neuron. This current may

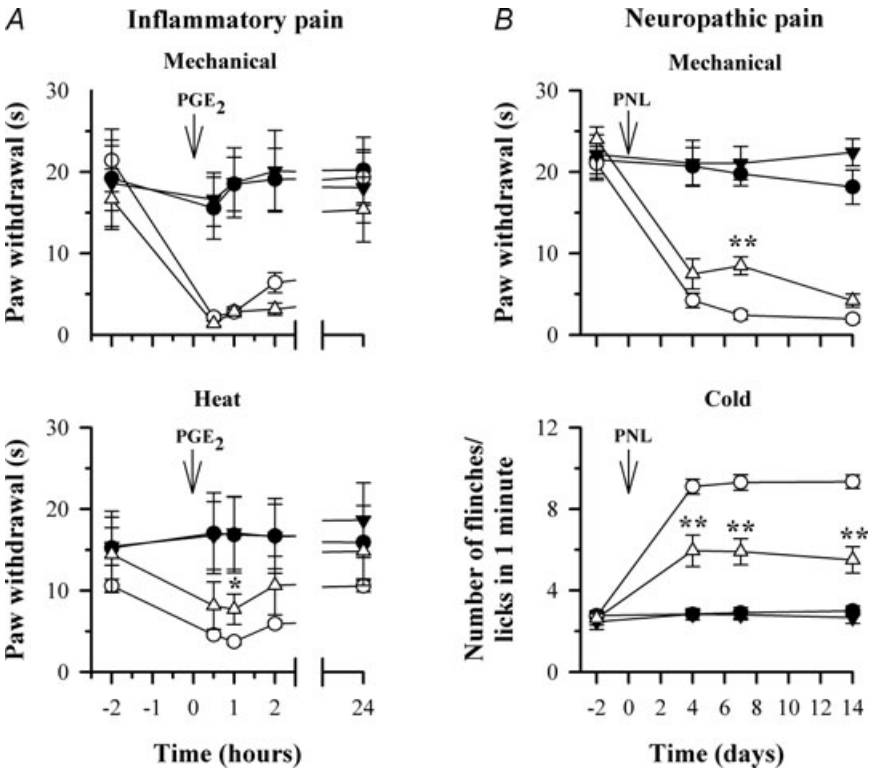

Figure 9. Hyperalgesia and allodynia in response to mechanical and thermal stimuli in inflammatory and neuropathic pain models in $HCN1^{+/+}$ and $HCN1^{-/-}$ mice
A, response to mechanical (2.5 g, upper panel) and radiant heat stimuli (lower panel) in $HCN1^{+/+}$ and $HCN1^{-/-}$ mice following PGE_2-induced inflammation. Symbols show the following: ●, $HCN1^{+/+}$, saline; ○, $HCN1^{+/+}$, PGE_2; ▼, $HCN1^{-/-}$, saline; △, $HCN1^{-/-}$, PGE_2. Different groups of $n = 5$ mice used for each time series. *B*, response to mechanical stimuli (upper panel ordinate shows paw withdrawal time to constant 2.5 g stimulus) and cold stimuli (lower panel, ordinate shows mean number of flinches/licks in 1 min following application of a drop of acetone) in $HCN1^{+/+}$ and $HCN1^{-/-}$ mice following partial sciatic nerve ligation (PNL). Symbols are: ●, $HCN1^{+/+}$, sham; ○, $HCN1^{+/+}$, operated; ▼, $HCN1^{-/-}$, sham; △, $HCN1^{-/-}$, operated. Same mice used for both panels; $n = 6$ for sham and $n = 10$ for operated. Tests of significance conducted between data obtained in $HCN1^{+/+}$ and $HCN1^{-/-}$ mice; $^*P < 0.05$, $^{**}P < 0.01$.

therefore be due to HCN3, which is more slowly activating than HCN1 and is insensitive to cAMP (Stieber *et al.* 2005). Thus in $HCN1^{+/+}$ mice and rats we propose that HCN1 is the only isoform expressed in the majority of large and medium-fast neurons, but that HCN1 forms heteromers with HCN3 in a minority of large and medium-fast neurons.

Most small neurons and about half of medium-sized neurons express a slowly activating I_h whose voltage activation is modulated by cAMP. I_h in these neurons was unaffected by deletion of HCN1 (Fig. 7, Table 2). Several lines of evidence suggest that HCN2 is likely to be a major contributor to I_h in these neurons. The activation time constant of I_h seen in these neurons resembles that of HCN2 (Santoro *et al.* 2000; Chen *et al.* 2001) rather than HCN4 (Seifert *et al.* 1999). In immunocytochemical and *in situ* hybridization studies HCN2 has been found to be strongly expressed in DRG neurons, while HCN4 is expressed at a low level (Moosmang *et al.* 2001; Chaplan *et al.* 2003; Tu *et al.* 2004; Matsuyoshi *et al.* 2006; Luo *et al.* 2007; Obreja *et al.* 2008). These considerations do not, however, explain why the time constants of I_h activation differ in these two groups of neurons (see Figs 4 and 6). HCN channels have been shown to form heteromers in expression systems (Chen *et al.* 2001; Ulens & Tytgat, 2001), and HCN2 may form heteromers with HCN4 in small neurons, which have the slowest time constants.

A final minor class of small neurons expresses an I_h which is fast-activating, with a time constant indistinguishable from that in large neurons, and is insensitive to cAMP. These properties are consistent with expression of HCN1, and in agreement with this no small neurons with fast-activating I_h were found in $HCN1^{-/-}$ mice (Fig. 7*F*). These small neurons with fast I_h also express the cold-sensitive ion channel TRPM8, as shown by their sensitivity to menthol, a specific agonist for TRPM8 (Fig. 5).

The role of HCN1 in inflammatory and neuropathic pain

We tested the effect of deleting HCN1 on both inflammatory hyperalgesia and neuropathic pain *in vivo*. We induced inflammatory hyperalgesia by injection of PGE_2, which induces robust inflammatory hyperalgesia *in vivo* (Taiwo *et al.* 1989). We used PGE_2 rather than a more commonly used inflammatory stimulus (such as carageenan) in order to allow direct comparisons with our *in vitro* studies. HCN1 is expressed in large neurons, which are often thought of as being non-nociceptive in function, but in fact a substantial proportion of the largest afferent fibres are nociceptors, amongst which are both mechanically sensitive and heat-sensitive nociceptors (20% of somatosensory neurons in rat, see Djouhri & Lawson, 2004; Fang *et al.* 2005). HCN1 does not appear to play a substantial role in either mechanical or heat hyperalgesia, however, because the substantial reduction in mechanical and heat threshold seen following injection of PGE_2 was unchanged in $HCN1^{-/-}$ mice (Fig. 9*A*).

Neuropathic pain is a widespread clinical problem, poorly treated by current drug therapies. Cold allodynia, an unpleasant sensation in response to normally non-noxious cold stimuli, is a particular problem in some forms of cancer chemotherapy, and is often a limiting factor in patients' ability to tolerate chemotherapy. Previous studies have suggested an important role for I_h in the initiation of action potentials in neuropathic pain (Chaplan *et al.* 2003). Continuous or burst firing in afferent nociceptors is likely to be a causative agent in the continuous pain, allodynia and hyperalgesia which are characteristic of neuropathic pain states (Kajander *et al.* 1992; Sheen & Chung, 1993).The I_h blocker ZD7288 reduces ectopic firing in sensory neurons and alleviates allodynia caused by nerve injury (Chaplan *et al.* 2003; Luo *et al.* 2007). In addition, a role for I_h in the hyper-excitability of damaged peripheral nerves has been proposed (Yao *et al.* 2003).

We examined a possible role for HCN1 in neuropathic pain by implementing in $HCN1^{+/+}$ and $HCN1^{-/-}$ littermates an experimental neuropathic pain model, in which neuropathic pain is induced by partial ligation of the sciatic nerve (Seltzer *et al.* 1990; Malmberg & Basbaum, 1998). Robust mechanical hyperalgesia and cold allodynia were observed 4 days post-operation and persisted for > 2 weeks (Fig. 9*B*). Deletion of HCN1 had little effect on mechanical hyperalgesia (Fig. 9*B*, top panel), implying that HCN1 plays little role in the generation of action potentials in the sensory endings responsible for the mechanical hyperalgesia in neuropathic pain.

A substantial and highly significant difference was observed in cold allodynia, however, which was more than halved by deleting HCN1 at all times tested. Detection of cold stimuli is mediated by a subpopulation of small-diameter DRG neurons (Reid & Flonta, 2001), which are unusual among small neurons in that a voltage- and time-dependent inward current is rapidly activated in response to hyperpolarizing current injection (Viana *et al.* 2002), consistent with expression of HCN1. In the present work we have identified in both rat and mouse neurons a subpopulation of small neurons with a fast-activating, cAMP-insensitive I_h, likely to correspond to the expression of HCN1, and we demonstrated in rat that these neurons are menthol sensitive and therefore express the cold-sensitive ion channel TRPM8 (Fig. 5). Repetitive firing in this population of small, cold-sensitive neurons in response to the steady inward current induced by a cold stimulus may therefore be promoted by the presence of HCN1, and thus would provide an explanation

for our observation that deletion of HCN1 substantially diminishes cold allodynia.

References

Akopian AN, Souslova V, England S, Okuse K, Ogata N, Ure J, Smith A, Kerr BJ, McMahon SB, Boyce S, Hill R, Stanfa LC, Dickenson AH & Wood JN (1999). The tetrodotoxin-resistant sodium channel SNS has a specialized function in pain pathways. *Nat Neurosci* **2**, 541–548.

Altomare C, Terragni B, Brioschi C, Milanesi R, Pagliuca C, Viscomi C, Moroni A, Baruscotti M & DiFrancesco D (2003). Heteromeric HCN1-HCN4 channels: a comparison with native pacemaker channels from the rabbit sinoatrial node. *J Physiol* **549**, 347–359.

Carlton SM, Lekan HA, Kim SH & Chung JM (1994). Behavioral manifestations of an experimental model for peripheral neuropathy produced by spinal nerve ligation in the primate. *Pain* **56**, 155–166.

Cesare P & McNaughton PA (1996). A novel heat-activated current in nociceptive neurons, and its sensitization by bradykinin. *Proc Natl Acad Sci U S A* **93**, 15435–15439.

Chan CS, Shigemoto R, Mercer JN & Surmeier DJ (2004). HCN2 and HCN1 channels govern the regularity of autonomous pacemaking and synaptic resetting in globus pallidus neurons. *J Neurosci* **24**, 9921–9932.

Chaplan SR, Guo HQ, Lee DH, Luo L, Liu C, Kuei C, Velumian AA, Butler MP, Brown SM & Dubin AE (2003). Neuronal hyperpolarization-activated pacemaker channels drive neuropathic pain. *J Neurosci* **23**, 1169–1178.

Chen S, Wang J & Siegelbaum SA (2001). Properties of hyperpolarization-activated pacemaker current defined by coassembly of HCN1 and HCN2 subunits and basal modulation by cyclic nucleotide. *J Gen Physiol* **117**, 491–504.

Choi Y, Yoon YW, Na HS, Kim SH & Chung JM (1994). Behavioral signs of ongoing pain and cold allodynia in a rat model of neuropathic pain. *Pain* **59**, 369–376.

DiFrancesco D (1993). Pacemaker mechanisms in cardiac tissue. *Annu Rev Physiol* **55**, 455–472.

DiFrancesco D & Ojeda C (1980). Properties of the current i_f in the sino-atrial node of the rabbit compared with those of the current i_{K2}, in Purkinje fibres. *J Physiol* **308**, 353–367.

DiFrancesco D & Tortora P (1991). Direct activation of cardiac pacemaker channels by intracellular cyclic AMP. *Nature* **351**, 145–147.

Djouhri L & Lawson SN (2004). Aβ-fiber nociceptive primary afferent neurons: a review of incidence and properties in relation to other afferent A-fiber neurons in mammals. *Brain Res Brain Res Rev* **46**, 131–145.

Doan TN, Stephans K, Ramirez AN, Glazebrook PA, Andresen MC & Kunze DL (2004). Differential distribution and function of hyperpolarization-activated channels in sensory neurons and mechanosensitive fibers. *J Neurosci* **24**, 3335–3343.

England S, Bevan S & Docherty RJ (1996). PGE_2 modulates the tetrodotoxin-resistant sodium current in neonatal rat dorsal root ganglion neurones via the cyclic AMP–protein kinase A cascade. *J Physiol* **495**, 429–440.

Evans AR, Vasko MR & Nicol GD (1999). The cAMP transduction cascade mediates the PGE_2-induced inhibition of potassium currents in rat sensory neurones. *J Physiol* **516**, 163–178.

Fang X, McMullan S, Lawson SN & Djouhri L (2005). Electrophysiological differences between nociceptive and non-nociceptive dorsal root ganglion neurones in the rat *in vivo*. *J Physiol* **565**, 927–943.

Fitzgerald EM, Okuse K, Wood JN, Dolphin AC & Moss SJ (1999). cAMP-dependent phosphorylation of the tetrodotoxin-resistant voltage-dependent sodium channel SNS. *J Physiol* **516**, 433–446.

Gold MS, Levine JD & Correa AM (1998). Modulation of TTX-R I_{Na} by PKC and PKA and their role in PGE_2-induced sensitization of rat sensory neurons *in vitro*. *J Neurosci* **18**, 10345–10355.

Gold MS, Reichling DB, Shuster MJ & Levine JD (1996). Hyperalgesic agents increase a tetrodotoxin-resistant Na^+ current in nociceptors. *Proc Natl Acad Sci U S A* **93**, 1108–1112.

Harper AA & Lawson SN (1985). Conduction velocity is related to morphological cell type in rat dorsal root ganglion neurones. *J Physiol* **359**, 31–46.

Harris NC & Constanti A (1995). Mechanism of block by ZD 7288 of the hyperpolarization-activated inward rectifying current in guinea pig substantia nigra neurons *in vitro*. *J Neurophysiol* **74**, 2366–2378.

Ingram SL & Williams JT (1994). Opioid inhibition of I_h via adenylyl cyclase. *Neuron* **13**, 179–186.

Ingram SL & Williams JT (1996). Modulation of the hyperpolarisation-activated current (I_h) by cyclic nucleotides in guinea-pig primary afferent neurons. *J Physiol* **492**, 97–106.

Jiang X, Zhang YH, Clark JD, Tempel BL & Nicol GD (2003). Prostaglandin E_2 inhibits the potassium current in sensory neurons from hyperalgesic Kv1.1 knockout mice. *Neuroscience* **119**, 65–72.

Kajander KC, Wakisaka S & Bennett GJ (1992). Spontaneous discharge originates in the dorsal root ganglion at the onset of a painful peripheral neuropathy in the rat. *Neurosci Lett* **138**, 225–228.

Kaupp UB & Seifert R (2001). Molecular diversity of pacemaker ion channels. *Annu Rev Physiol* **63**, 235–257.

Kerr BJ, Souslova V, McMahon SB & Wood JN (2001). A role for the TTX-resistant sodium channel Nav 1.8 in NGF-induced hyperalgesia, but not neuropathic pain. *Neuroreport* **12**, 3077–3080.

Komagiri Y & Kitamura N (2003). Effect of intracellular dialysis of ATP on the hyperpolarization-activated cation current in rat dorsal root ganglion neurons. *J Neurophysiol* **90**, 2115–2122.

Lawson SN (2002). Phenotype and function of somatic primary afferent nociceptive neurones with C-, Aδ- or Aα/β-fibres. *Exp Physiol* **87**, 239–244.

Lopshire JC & Nicol GD (1998). The cAMP transduction cascade mediates the prostaglandin E_2 enhancement of the capsaicin-elicited current in rat sensory neurons: whole-cell and single-channel studies. *J Neurosci* **18**, 6081–6092.

Ludwig A, Budde T, Stieber J, Moosmang S, Wahl C, Holthoff K, Langebartels A, Wotjak C, Munsch T, Zong X, Feil S, Feil R, Lancel M, Chien KR, Konnerth A, Pape HC, Biel M & Hofmann F (2003). Absence epilepsy and sinus dysrhythmia in mice lacking the pacemaker channel HCN2. *EMBO J* **22**, 216–224.

Luo L, Chang L, Brown SM, Ao H, Lee DH, Higuera ES, Dubin AE & Chaplan SR (2007). Role of peripheral hyperpolarization-activated cyclic nucleotide-modulated channel pacemaker channels in acute and chronic pain models in the rat. *Neuroscience* **144**, 1477–1485.

McKemy DD, Neuhausser WM & Julius D (2002). Identification of a cold receptor reveals a general role for TRP channels in thermosensation. *Nature* **416**, 52–58.

Magistretti J, Mantegazza M, de Curtis M & Wanke E (1998). Modalities of distortion of physiological voltage signals by patch-clamp amplifiers: a modeling study. *Biophys J* **74**, 831–842.

Malmberg AB & Basbaum AI (1998). Partial sciatic nerve injury in the mouse as a model of neuropathic pain: behavioral and neuroanatomical correlates. *Pain* **76**, 215–222.

Matsuyoshi H, Masuda N, Chancellor MB, Erickson VL, Hirao Y, de Groat WC, Wanaka A & Yoshimura N (2006). Expression of hyperpolarization-activated cyclic nucleotide-gated cation channels in rat dorsal root ganglion neurons innervating urinary bladder. *Brain Res* **1119**, 115–123.

Mo ZL & Davis RL (1997). Heterogeneous voltage dependence of inward rectifier currents in spiral ganglion neurons. *J Neurophysiol* **78**, 3019–3027.

Moosmang S, Stieber J, Zong X, Biel M, Hofmann F & Ludwig A (2001). Cellular expression and functional characterization of four hyperpolarization-activated pacemaker channels in cardiac and neuronal tissues. *Eur J Biochem* **268**, 1646–1652.

Nicol GD, Vasko MR & Evans AR (1997). Prostaglandins suppress an outward potassium current in embryonic rat sensory neurons. *J Neurophysiol* **77**, 167–176.

Nolan MF, Malleret G, Lee KH, Gibbs E, Dudman JT, Santoro B, Yin D, Thompson RF, Siegelbaum SA, Kandel ER & Morozov A (2003). The hyperpolarization-activated HCN1 channel is important for motor learning and neuronal integration by cerebellar Purkinje cells. *Cell* **115**, 551–564.

Obreja O, Klusch A, Ponelies N, Schmelz M & Petersen M (2008). A subpopulation of capsaicin-sensitive porcine dorsal root ganglion neurons is lacking hyperpolarization-activated cyclic nucleotide-gated channels. *Eur J Pain* **12**, 775–789.

Pape HC (1996). Queer current and pacemaker: the hyperpolarization-activated cation current in neurons. *Annu Rev Physiol* **58**, 299–327.

Pape HC & McCormick DA (1989). Noradrenaline and serotonin selectively modulate thalamic burst firing by enhancing a hyperpolarization-activated cation current. *Nature* **340**, 715–718.

Reid G & Flonta ML (2001). Cold current in thermoreceptive neurons. *Nature* **413**, 480.

Santoro B, Chen S, Luthi A, Pavlidis P, Shumyatsky GP, Tibbs GR & Siegelbaum SA (2000). Molecular and functional heterogeneity of hyperpolarization-activated pacemaker channels in the mouse CNS. *J Neurosci* **20**, 5264–5275.

Scroggs RS, Todorovic SM, Anderson EG & Fox AP (1994). Variation in IH, IIR, and ILEAK between acutely isolated adult rat dorsal root ganglion neurons of different size. *J Neurophysiol* **71**, 271–279.

Seifert R, Scholten A, Gauss R, Mincheva A, Lichter P & Kaupp UB (1999). Molecular characterization of a slowly gating human hyperpolarization-activated channel predominantly expressed in thalamus, heart, and testis. *Proc Natl Acad Sci U S A* **96**, 9391–9396.

Seltzer Z, Dubner R & Shir Y (1990). A novel behavioral model of neuropathic pain disorders produced in rats by partial sciatic nerve injury. *Pain* **43**, 205–218.

Sheen K & Chung JM (1993). Signs of neuropathic pain depend on signals from injured nerve fibers in a rat model. *Brain Res* **610**, 62–68.

Sherrington CS (1906). *The Integrative Action of the Nervous System.* Scribner, New York.

Snider WD & McMahon SB (1998). Tackling pain at the source: New ideas about nociceptors. *Neuron* **20**, 629–632.

Southan AP, Morris NP, Stephens GJ & Robertson B (2000). Hyperpolarization-activated currents in presynaptic terminals of mouse cerebellar basket cells. *J Physiol* **526**, 91–97.

Stieber J, Stockl G, Herrmann S, Hassfurth B & Hofmann F (2005). Functional expression of the human HCN3 channel. *J Biol Chem* **280**, 34635–34643.

Stucky CL & Lewin GR (1999). Isolectin B_4-positive and -negative nociceptors are functionally distinct. *J Neurosci* **19**, 6497–6505.

Taiwo YO, Bjerknes LK, Goetzl EJ & Levine JD (1989). Mediation of primary afferent peripheral hyperalgesia by the cAMP second messenger system. *Neuroscience* **32**, 577–580.

Tu H, Deng L, Sun Q, Yao L, Han JS & Wan Y (2004). Hyperpolarization-activated, cyclic nucleotide-gated cation channels: roles in the differential electrophysiological properties of rat primary afferent neurons. *J Neurosci Res* **76**, 713–722.

Ulens C & Tytgat J (2001). Functional heteromerization of HCN1 and HCN2 pacemaker channels. *J Biol Chem* **276**, 6069–6072.

Viana F, de la Peña E & Belmonte C (2002). Specificity of cold thermotransduction is determined by differential ionic channel expression. *Nat Neurosci* **5**, 254–260.

Yagi J & Sumino R (1998). Inhibition of a hyperpolarization-activated current by clonidine in rat dorsal root ganglion neurons. *J Neurophysiol* **80**, 1094–1104.

Yao H, Donnelly DF, Ma C & LaMotte RH (2003). Upregulation of the hyperpolarization-activated cation current after chronic compression of the dorsal root ganglion. *J Neurosci* **23**, 2069–2074.

Yoshida S & Matsuda Y (1979). Studies on sensory neurons of the mouse with intracellular-recording and horseradish peroxidase-injection techniques. *J Neurophysiol* **42**, 1134–1145.

Acknowledgements

We thank Carlos Belmonte and Felix Viana for helpful discussions, Xuming Zhang and Esther Berrocoso for comments

on the manuscript, and we thank Sue Boyce and Gillian Gourlay for assistance with the behavioural models. This work was supported by the BBSRC. The generation of HCN1$^{-/-}$ mice was carried out in collaboration with Lexicon Pharmaceuticals Inc.

Commercial interest. Dr Adrian Mason, a joint author of this manuscript, is an employee of Schering-Plough Corporation, currently pursuing a drug discovery programme in the area of HCN ion channels.

Supplemental material

Online supplemental material for this paper can be accessed at: http://jp.physoc.org/cgi/content/full/jphysiol.2008.163154/DC1